

# 62.5-GHz Phased-Array Channel Sounder for Double-Directional Angle Estimation

Peter Papazian<sup>1</sup>, Derek Caudill<sup>1</sup>, Camillo Gentile<sup>2</sup>, Jack Chuang<sup>2</sup>, Nada Golmie<sup>2</sup>

<sup>1</sup> Communications Technology Laboratory, NIST, Boulder, Colorado, USA, [peter.papazian@nist.gov](mailto:peter.papazian@nist.gov), [derek.caudill@nist.gov](mailto:derek.caudill@nist.gov)

<sup>2</sup> Communications Technology Laboratory, NIST, Gaithersburg, Maryland, USA, [camillo.gentile@nist.gov](mailto:camillo.gentile@nist.gov), [jack.chung@nist.gov](mailto:jack.chung@nist.gov)

*Abstract*— The paper describes implementation of phased array antennas for use in a wideband channel sounding system. The antennas are 62.5 GHz prototypes, utilizing SiGe chips on a printed circuit-board. Each board consists of two 16-element series-fed patch array arrays with separate RF ports and IF sections. Each 16-element array can scan  $\pm 45^\circ$  with a fixed elevation beamwidth. The receiver uses 4 antenna boards oriented at  $90^\circ$  to enable omni direction coverage when scanning. The transmitter consists of two array-boards also implemented at  $90^\circ$  which allows  $180^\circ$  transmitter coverage. Direction of departure and direction of arrival multipath measurements are made using Rubidium clocks at both the transmitter and receiver and a timing synchronization system to coordinate the receiver scanning with the transmitter scanning and the data acquisition system. The objective of the system is to collect directional propagation data utilizing prototype phased array boards and tracking algorithms at millimeter wave frequencies.

*Index Terms*—channel sounder, phased-array, millimeter waves, multipath tracking.

## I. INTRODUCTION

Advances in phased array antenna technology is important for 5G communication systems operating at millimeter wave frequencies. Highly directional phased array antennas with 20–40 dBi gain will compensate for the higher path loss allowing link distances of several hundred meters. Since their associated beamwidth will only lie between  $3^\circ$ – $15^\circ$ , to provide an omnidirectional field-of-view, they must be steered towards the angle-of-departure (AoD) and angle-of-arrival (AoA) of any viable propagation paths between the respective transmitter (TX) and receiver (RX). Hence, it is essential for 5G channel models to capture the *double-directionality* of the channel [1].

A key capability of 5G systems and sounder will be the ability to track multipath components in LOS and NLOS conditions. Typical channel sounder deployed to date have not used phased array antennas which limited their ability to track multipath and changes in AoD and AoA in dynamic environments [2,3,4,5,6,7,8,9,10]. To investigate phased array antenna capabilities, and to develop tracking algorithms for narrow beam antennas with electronic scanning capability NIST is developing a phased array channel sounder.

Phased-array antennas have the additional benefit of half-wavelength spacing between elements, like virtual arrays, making coherent phase combination to deliver high angular resolution of multipath components (MPCs). Given the number of elements per array, typically 16–64, they also have gain above 25 dBi. Finally, they can have bandwidths up to 2 GHz and have switch time on the order of microseconds. These antenna features will help provide data for realistic channel models which should be applicable to 5G systems design.

The rest of the paper is organized as follows: In Section II, we describe our phased-array antenna boards and the transmitter and receiver front ends driving the boards, followed by Section III describing the OTA system calibration as well as the antenna pattern measurements and system timing stability. In Section IV, we describe pre-distortion filter data. This method has been used in our switched array systems [11] to improve the dynamic range of the measured impulse response and is now extended to the phased array system. Lastly, we provide a conclusion and avenues for further research.

## II. SYSTEM ARCHITECTURE

### A. Phased Array Antennas

Details of phased-array antennas in our system are described in [12], so our intention here is to highlight their main features. As displayed in Figure 1a, the boards are composed from  $8 \times 32$  microstrip patch antennas spaced at  $0.54 \lambda$  and polarized in the elevation plane only. Their center frequency is 62.5 GHz ( $\lambda = 4.8$  mm) with a 2-GHz passband. The only difference from the citation is that our boards have two ports – not just one – splitting them into two  $8 \times 16$  arrays allows enhanced flexibility in implementation. The ports have a companion mixer for up/down-conversion. The mixers assembly with integral LO frequency doublers are in the lower section of the assembly in Figure 1b and displayed on the block diagrams Figure 2. The eight antenna elements per array column have a common amplifier and phase shifter, so steering is in the azimuth plane only. The purpose of multiple elements is to increase gain by limiting beamwidth in the elevation plane. Boresight gain is 26.1 dBi. The azimuth beamwidth is  $5.6^\circ$  while the elevation beamwidth is  $12^\circ$ .

The scan range of each array is  $\pm 45^\circ$ , hence four boards arranged at right angles is necessary to obtain an omnidirectional field-of-view at the receiver. It is critical for

the receiver to “see” from all directions since it will be mounted on a mobile robot. The condition is somewhat relaxed at the transmitter because it is fixed on a tripod and emission from the backside is less important. As such, the transmitter only has two boards to reduce the channel sweep time. The boards were also arranged at right angles for a combined 180° field-of-view.

### B. Transmitter Section

At the transmitter, an arbitrary waveform generator synthesizes a repeating BPSK-modulated pseudorandom-noise (PN). The code has 2047 chips with 1-ns chip length. The code is generated at 2.5 GHz intermediate frequency (IF), followed by a bandpass filter with 2-GHz null-to-null bandwidth to truncate the signal beyond its first lobe to avoid out of band interference. The signal is then upconverted to 62.5 GHz and transmitted. Four AWG channels are available allowing independent operation of each RF port in regard to coding and beam steering.

### C. Receiver Section

The received signal is down-converted to IF and then directly digitized and subsequently correlated with the known code, yielding the complex channel impulse response.

Using Rubidium clocks, low phase noise oscillators and a timing synchronization circuit, the system can be switched through RX-TX beam pairs with a time deviation of  $<2$ ps between multipath channels. In our nominal receiver implementation, one RF port is operational per antenna board: the port is scanned across  $\pm 45^\circ$  with  $5.6^\circ$  increments – equivalent to the width of the beam at boresight so that the synthesized antenna pattern of all beams covers the omnidirectional space at the RX and 180 degrees at the TX. This requires 17 RX scanning angles per board or a total of 2312 (68 x 34) RX-TX beam pairs. The digitizer has eight channels and each port on the antenna array board has its own RF section with an IF output Figure 1. This allows each receiver port to be recorded simultaneously; in addition, orthogonal PN codes can be sent to the transmitter boards by using 2 AWG channels. This allows multiple transmitter beams to be scanned simultaneously; together, this reduces the total scan time by a factor of eight. Given that switch period to change phase states using the on-board SPI interface is  $36 \mu\text{s}$  plus  $4 \mu\text{s}$  to record two code words, the minimum time for a full channel sweep is  $\Delta t = 11.6 \text{ ms}$ .

For each beam pair, the received signal is down-converted back to IF and then directly digitized. The digitized signal is then match filtered with the known code, yielding the complex channel impulse response of the beam pair. The advantage of direct digitization is that the match filtering is done in post-processing so that the channel can be sampled at  $\Delta t$ , corresponding to a maximum measurable Doppler shift of

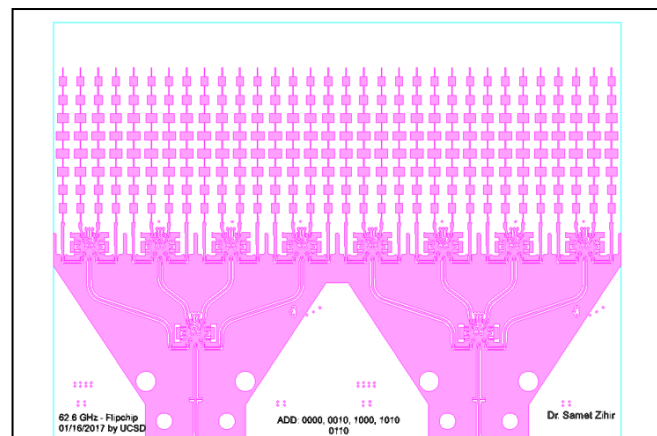


Figure 1(a) 62.5 GHz phased-array antenna board. The board contains two 8 x 16 arrays with separate feeds.

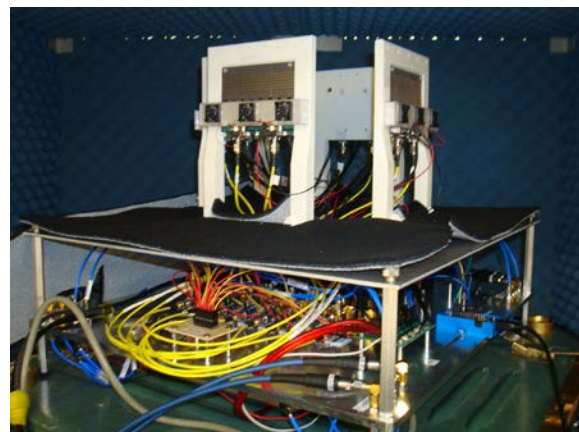


Figure 1(b). Receiver section. Four antenna-arrays boards, each with  $\pm 45^\circ$  azimuth scan range, are mounted at right angles in order to provide an omnidirectional field-of-view at the receiver.

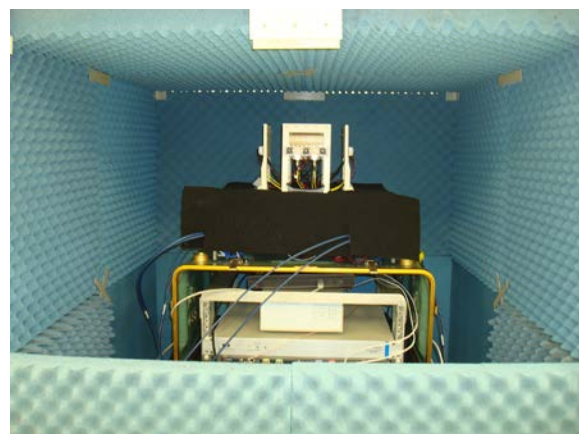


Figure 1(c). Receiver section mounted in anechoic chamber for array calibration and pre-distortion filter measurements.

43.3 Hz. Doppler shift is related to  $f_c$  and relative velocity between the transceivers,  $v$ , using,  $|v|_{\text{max}} = \frac{|\Delta f|_{\text{max}}}{f_c} \cdot c$ , where  $c$  is the speed of light. This means that we can operate our mobile robot up to a maximum speed of  $|v|_{\text{max}} = 0.2 \text{ m/s}$ .

To deal with higher mobility scenarios, both ports per board are operational on separate channels to split the number of scans per board, halving the scan time. To further decrease the scan time, the array size per port is reduced to  $8 \times 6$  by activating only 12 of the 32 columns. Besides reducing the SPI-switch period to  $27 \mu\text{s}$ , this moreover widens the beam to  $15^\circ$ , reducing the total number of scans to three per port. This implies unique PN codes at four transmitter ports. Ultimately, the scan time is reduced to 2 ms such that a maximum closing speed of 1.2 m/s can be sustained, however at the expense of lower signal-to-noise ratio given the reduced gain (4.3 dB per array) and the greater interference due to multiple codes as well as reduction in angular precision due to the wider beamwidths.

Due to the switching speeds of our prototype arrays this will make Doppler measurements only possible when beam tracking. Consequently, acquisitions will be separated into MPC identification and beam tracking modes.

### III. System Calibration

To achieve optimal channel sounding performance, the non-ideal effects of each system component, from the transmitter and receiver sections of each array board, must be characterized and compensated for.

#### A. Computation of the Array Beamforming Weights

Electrical steering of the arrays is accomplished by programming the complex weights of the array columns through the SPI controller. Each weight is composed from a complex multiplication of magnitude and phase values – 5 bits for the phase state and 4 bits for the magnitude state – that are programmed independently. As can be seen from Figure 1a, each array also has a common feed for groups of four adjacent elements arranged in a Wilkinson network structure. The feed affects the signal passing through, so the magnitude and phase values of the common feed is added to the column weight. Although each state has a pre-defined nominal value, the values can vary significantly between arrays due to different electrical-path lengths and other non-ideal effects. As such, the amplitude and phase values must be accurately characterized for each programmable setting of the array states to optimize the array patterns.

A vector network analyzer (VNA) and mm-Wave frequency extension modules were utilized for characterization of the amplitude and phase state of the array. The measurements were conducted in an anechoic chamber with port1 of the VNA connected to a horn antenna and port 2 connected to the array. The antennas were pointed at each other at boresight at 3.323 meters. A CW signal at the center frequency of the array was then transmitted from the horn antenna. Then S21 measurements were recorded at all the gain and phase states

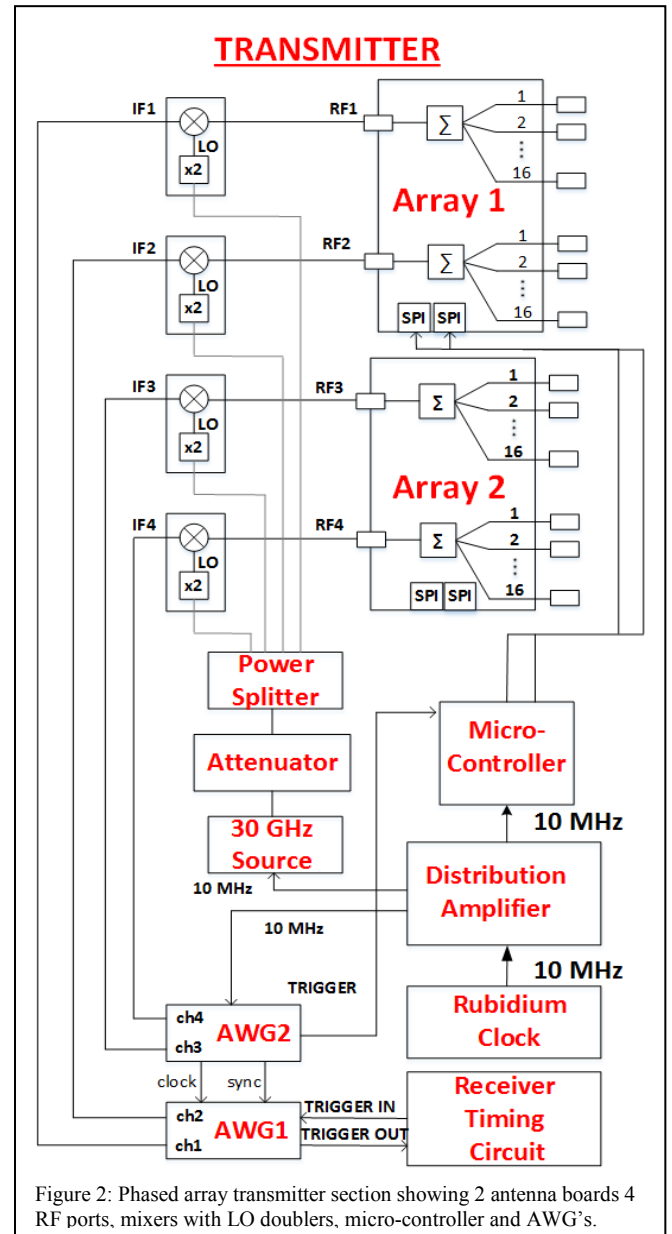


Figure 2: Phased array transmitter section showing 2 antenna boards 4 RF ports, mixers with LO doublers, micro-controller and AWG's.

of the array. In all, each array had a total of 1024 states for the transmit mode and another 1024 states for receive mode.

With the complex values of the states known, the optimal selection of phase and magnitude states were determined across the columns for each scan angle. In our implementation, the first column was selected arbitrarily as the reference column and each of its phase states constituted a unique candidate on the list. For each candidate, the desired phase of the  $i^{\text{th}}$  column was computed as

$$\phi_i = \frac{2\pi}{\lambda} d_i \sin\theta_0 + \phi_1, \quad (1)$$

where  $\phi_1$  denotes the phase value of the first column,  $d_i$  the distance of the  $i^{\text{th}}$  column from the first column, and  $\theta_0$  the

desired scan angle. The phase state whose value that was closest to the desired value,  $\phi_i$  – i.e., the phase value that rendered the smallest error – was selected per column. The candidates were subsequently ranked according to the average error across the array columns (elements) and the optimal one was chosen.

### B. Measurement of Array Antenna Patterns

Once the array's beamforming weights were computed, its resultant complex antenna patterns were measured for all scan angles. The arrays on the receiver and transmitter sections were measured separately. First, we considered the receiver. Similar to the setup in Section III.A, a horn antenna was pointed towards the receiver section. However, in this setup the VNA was not used; rather, the PN sequence was preferred to capture the wideband response of the arrays to the actual transmitted signal. To measure the array azimuthal pattern the receiver was placed on a rotating table.

Let  $\hat{\theta}^R$  denote the azimuth angle of the receiver array relative to boresight of the transmitting horn. The array pattern was first electronically steered towards angle  $\theta_i^R = \hat{\theta}^R - 45^\circ \dots \hat{\theta}^R + 45^\circ$  at  $5.6^\circ$  increments, for a total  $i = 1 \dots 17$  scan angles. For each scan angle, the rotator was used to align the boresight of the steered pattern with the boresight of the horn. The purpose of mechanical rotation was to characterize the sidelobes of the antenna pattern for each electronic scan angle. Accordingly, the rotator was stepped out from  $\theta_i^R = \hat{\theta}_i^R - 45^\circ \dots \hat{\theta}_i^R + 45^\circ$  at  $0.25^\circ$  increments. The small mechanical scan angle increment is import for subsequent measurements of the AOA and AOD. As will be seen in a sequel to this paper the cost function of AOA and AOD estimation is sensitive to small changes in signal amplitude versus angle so this small mechanical increment was used for determining patterns at all scan angles and all antenna array boards at both the transmitter and the receiver.

Figure 3 shows the results using optimal weights for a uniform array and the results using an 8dB  $\cos^2(\phi)$  taper. The tapering reduced side-lobe levels between 5-7 dB while increasing the beamwidth by 1 degree. It also increased the peak of the main beam by 4 dB.

### C. Time stability

The timing stability of the phased array channel sounder can be analyzed using Equation 2 [13,14,15,16],

$$x(t) = x_0 + y_0 t + \frac{1}{2} D t^2 + \sigma_x(t). \quad (2)$$

Where:  $x(t)$  is the timing error,  $x_0$  is the initial time offset,  $y_0 = \Delta f/f$ , is a constant fractional frequency offset,  $D$  is the frequency drift rate ("aging") of the rubidium cell, and  $\sigma_x(t)$  is random noise or an environmentally induced time deviation.

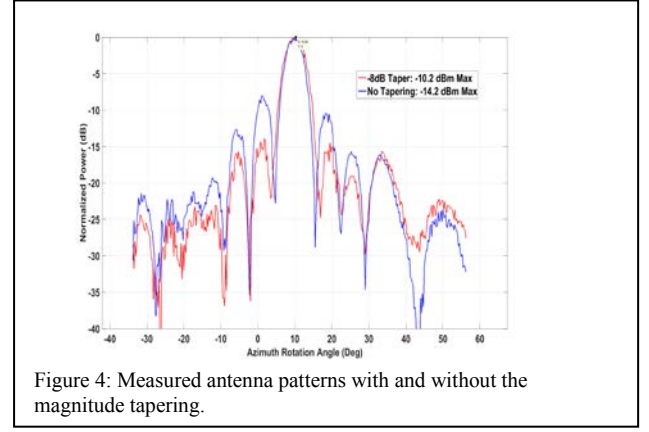


Figure 4: Measured antenna patterns with and without the magnitude tapering.

$\sigma_x(t)$  can be measured using an equispaced time series of time-interval measurements,  $x_i = t_{m,i} - t_{i,i}$  where  $m,i$  denotes measured signal  $i^{th}$  point and  $i,i$  denotes ideal signal,  $i^{th}$  point. Time deviation then be calculated using the modified Allan Variance which is a common measure of time stability using Equation 3.

$$\sqrt{\sigma_x^2(t) = \frac{\tau^2}{3} \text{Mod} \sigma_y^2(t)} \quad (3)$$

Figure 4 shows two measurements of  $x_i(t)$  for the channel sounder system at its IF after up and down conversion. When using one Rubidium clock as time reference for both systems (red curve), the timing error  $t_i$ , has a constant average value of zero  $ps$  for 20  $ms$ . The time deviation (TDEV) is 0.38  $ps$ .

Using two clocks for the untethered mode of operation (blue data), we see a constant slope of  $-3.5e-9$  over the 20  $ms$  interval. This is due to the frequency offset between the two clocks after synchronization. It can be removed by subtracting this average slope from the relative impulse response or MPC timing during an acquisition. TDEV is then used to estimate timing errors. The untethered timing errors now have a constant average value of 0  $ps$ . TDEV for the blue data is estimated to be 0.25  $ps$ .

Since TDEV for tethered and untethered operation are  $<1$   $ps$  the timing and phase errors for both tethered and untethered operation will be similar given adequate system synchronization and data processing methods.

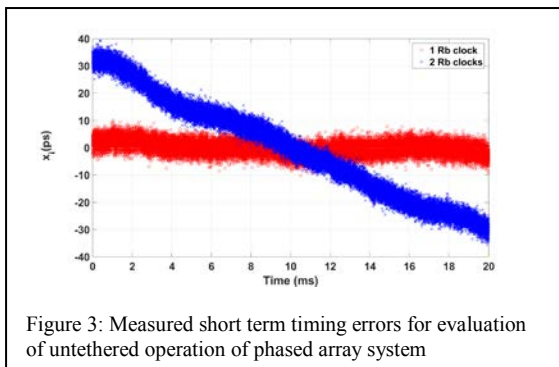


Figure 3: Measured short term timing errors for evaluation of untethered operation of phased array system

#### IV. PREDISITORION FILTERS

Predistortion filtering is used to remove systematic system level distortions caused in the RF and IF sections of the system. The procedure for calculating these filters is described in a previous paper [11]. It was found that the filters did not change as a function of scanning angle for an individual RF section on each antenna board. As such these filters were calculated at the boresight steering angle and then applied to each RF section for all steering angles. A representative response is shown in Figure 4. This figure shows the effect of the filter at short delay times for 1-3 iterations of the filtering process. It shows a reduction of spurious multipath components in the PDP from a level of -30dB relative to the peak of the PDP down to -50dB. It also reduced spurious signals at longer delays. These filters are complex-valued so they also effect the phase response of the MPC's which will be discussed in a sequel to this paper.

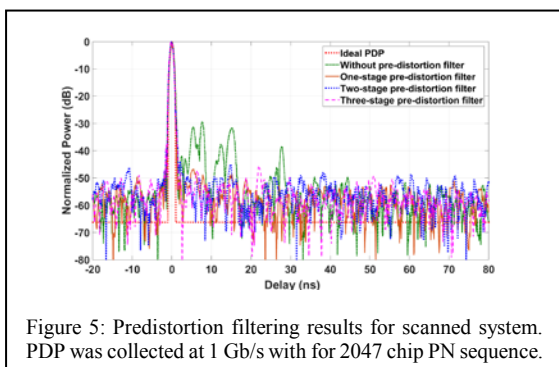


Figure 5: Predistortion filtering results for scanned system. PDP was collected at 1 Gb/s with for 2047 chip PN sequence.

#### V. CONCLUSIONS AND FURTHER WORK

The essential requirements for 5G channel sounding are high directional gain, double-directional scanning capabilities, high angular resolution, ultra-wide bandwidth, and fast sweep time. In this paper, we presented a 60-GHz phased-array-antenna system that meets those requirements. We described over-the-air techniques to calibrate the antennas and measure their patterns, as well as calibrate the frequency response to maximize the dynamic range of the system.

We hope to implement and field the system at 60 GHz to test tracking algorithms first indoors and then outdoors. We also plan to develop a 28 GHz system using dual polarized patch arrays.

#### REFERENCES

- [1] Huang, Jie, Yu Liu, Cheng-Xiang Wang, Jian Sun, and Hailin Xiao. "5G Millimeter Wave Channel Sounders, Measurements, and Models: Recent Developments and Future Challenges." *IEEE Communications Magazine* (2018).
- [2] J. Senic, C. Gentile, P.B. Papazian, et al., "Analysis of E-band Path Loss and Propagation Mechanisms in the Indoor Environment," *IEEE Trans. on Antennas and Propagation*, vol. 65, no. 2, pp. 6562 – 6573, Dec. 2017.
- [3] S. Hur, Y.-J. Cho, J. Lee, et al., "Synchronous Channel Sounder Using Horn Antenna and Indoor Measurements on 28 GHz," *IEEE Black Sea Conf.*, May 2014.
- [4] J.-J. Park, J. Liang, J. Lee, et al., "Millimeter-Wave Channel Model Parameters for Urban Microcellular Environment Based on 28 and 38 GHz Measurements," *IEEE PIMRC*, Sept. 2016.
- [5] S.A. Saberali and N.C. Beaulieu, "New expressions for TWDP fading statistics," *IEEE Wireless Communication Letters*, vol. 2, no. 6, pp. 643-646, Dec. 2013.
- [6] B.N. Lia and D. G. Michelson, "Characterization of Multipath Persistence in Device-to-Device Scenarios at 30 GHz," *IEEE GLOBECOM*, Dec. 2016.
- [7] Dupleich, D., Fuschini, F., Mueller, R., et al., "Directional characterization of the 60 GHz indoor-office channel." In *General Assembly and Scientific Symposium (URSI GASS), 2014 XXXIth URSI*, pp. 1-4. IEEE, 2014.
- [8] D. Dupleich, J. Luo, S. Haefner, et al., "A Hybrid Polarimetric Wide-Band Beam-former Architecture for 5G mm-Wave Communications," *IEEE Workshop on Smart Antennas*, pp. 1-8, March 2016.
- [9] Mbugua AW, Fan W, Ji Y, Pedersen GF. "Millimeter Wave Multi-user Performance Evaluation Based on Measured Channels with Virtual Antenna Array Channel Sounder." *IEEE Access*. 2018 Jan 1.
- [10] Rupakula, B., Nafe, A., Zahir, S., et al., (2018). "63.5-65.5-GHz Transmit/Receive Phased-Array Communication Link With 0.5-2 Gb/s at 100-800 m and  $\pm 50^\circ$  Scan Angles." *IEEE Trans. on Microwave Theory and Techniques*, (99), 1-13.
- [11] R. Sun, P.B. Papazian, J. Senic, et al., "Design and Calibration of a Double-directional 60 GHz Channel Sounder for Multipath Component Tracking," *IEEE EuCAP*, March 2017.
- [12] B. Rupakula, A. Nafe, S. Zahir, Y. Wang, T. Lin and G. Rebeiz, "63.5–65.5-GHz Transmit/Receive Phased-Array Communication Link With 0.5–2 Gb/s at 100–800 m and  $\pm 50^\circ$  Scan Angles," in *IEEE Transactions on Microwave Theory and Techniques*, vol. 66, no. 9, pp. 4108-4120, Sept. 2018.
- [13] W.J. Riley, "Handbook of Frequency Stability Analysis", *NIST Special Publication 1065*, pp19, July 2008.
- [14] W. Allan, D. D. Davis, J. Levine, M. A. Weiss, N. Hironaka, D. Okayama, "New inexpensive frequency calibration service from Natl. Inst. Stand. Technol.," *Proc. 44th Freq. Cont. Symp.*, pp. 107-116. June 1990.
- [15] D.W. Allan, M.A. Weiss, J. L. Jespersen, "A frequency-domain view of time-domain characterization of clocks and time and frequency distribution systems," *Proc. 45th Freq. Cont. Symp.*, pp. 667-678, May 1991.
- [16] D.W. Allan, M.A. Weiss, J. L. Jespersen, "A frequency-domain view of time-domain characterization of clocks and time and frequency distribution systems," *Proc. 45th Freq. Cont. Symp.*, pp. 667-678, May 1991.